Journal of
Mechanics of
Materials and Structures

**PERFORMANCE AND FAILURE OF METAL SANDWICH PLATES
SUBJECTED TO SHOCK LOADING**

Ashkan Vaziri, Zhenyu Xue and John W. Hutchinson

PERFORMANCE AND FAILURE OF METAL SANDWICH PLATES SUBJECTED TO SHOCK LOADING

ASHKAN VAZIRI, ZHENYU XUE AND JOHN W. HUTCHINSON

The deflection and fracture of metal sandwich plates subjected to intense uniform impulsive pressure loads are studied for plates made of four steels representing a wide range of strength, strain hardening and ductility. Sandwich plates with both square honeycomb cores and folded plate cores are considered. The primary fracture modes of the sandwich plates are necking and subsequent tearing of the face sheets and webs and shear delamination of the core webs from the faces. Plates with square honeycomb cores have higher damage tolerance than those with folded plate cores in that they can withstand much larger loads above those at which the first signs of fracture appear. The trade-off between strength and ductility in plate performance is illustrated.

1. Introduction

All-metal sandwich plates perform better than solid plates of equal mass in resisting high intensity dynamic pressure loads, especially in water environments where sandwich construction benefits from fluid-structure interaction to reduce momentum transfer [Fleck and Deshpande 2004; Xue and Hutchinson 2004; Hutchinson and Xue 2005; Liang et al. 2007]. Whether the plate is monolithic or a sandwich, combinations of high ductility and high strength promote good performance. Assuming the material is sufficiently ductile to survive an intense blast, the ratio of maximum deflection δ to plate half-width L scales as [Xue and Hutchinson 2004]

$$\frac{\delta}{L} \propto \frac{I}{M\sqrt{\sigma_Y/\rho}}, \tag{1}$$

where I is the impulsive momentum/area transferred to the plate, ρ is the material density, σ_Y is the material yield stress, and M is the mass/area of the plate. To minimize δ/L for plates of a given M subjected to a given I, materials with high specific strength, σ_Y/ρ, are clearly preferred, assuming adequate ductility.

When metal plates are subjected to shock loading, various failure modes occur depending on the plate design and spatial details of the impulsive loading. For a solid plate, the two primary competing modes are failure at the supports and ductile tearing in the interior regions of the plate away from the supports. Failure at a support can be precipitated by tensile necking followed by ductile tearing, or it may take the form of a highly localized through-thickness shear failure [Nahshon et al. 2007]. Failure at supports and interior ductile tearing are also failure modes for face sheets of sandwich plates. Under intense impulsive loads, core webs will generally undergo extensive plastic buckling under compression or shear. In the

present context, buckling is regarded as a deformation mode and not a failure mode. However, extensive buckling can promote failure in either the core or the faces. Core failures occur as web tearing or as shear fracture at welded joints. Core failures do not necessarily imply ultimate failure since a sandwich plate can still have substantial residual strength afterward.

In this paper, we explore the role of material choice on plate performance against impulsive loads by evaluating failure modes and ultimate failure for two sandwich plate designs, one with a square honeycomb core and the other with a folded plate core. Four types of steel have been considered to delineate the roles of strength, strain hardening and ductility. The material description used here is based on the conventional J_2 plasticity constitutive relation with fracture imposed when the effective plastic strain reaches a critical value that may depend on the mean stress. This approach, coupled with element deletion when the failure criterion is met, has been widely used for finite element computations based on the early contributions to ductile fracture of Hancock and Mackenzie [1976] and subsequent work of Johnson and Cook [1983]. We characterize steels by yield strength, strain hardening, and ductility as a function of mean-stress. We describe failure modes and compute deflections and maximum sustainable impulses.

2. Plates and loading specifications

Following several earlier studies [Xue and Hutchinson 2004; Vaziri et al. 2006; Vaziri and Hutchinson 2007], we model the plates as infinite in one direction and of width $2L$ in the other, with clamped conditions along the two edges. Solid plates have thickness h and mass/area $M = \rho h$. The two types of sandwich plates considered are shown in Figure 1: one with a square honeycomb core and the other with a folded plate core running perpendicular to the clamped edges. Figure 1 also depicts periodic units employed in the finite element models. Both core topologies have height H, web thickness t, and face sheet thickness h_f (the top and bottom faces of the sandwich plates have equal thickness). The square honeycomb core has web spacing B. The folded plate core has an inclination angle α such that the spacing of the folds is $B = t/\sin\alpha + H/\tan\alpha$. Denoting the relative density of the core (that is, the volume fraction of the core occupied by the webs) by f_c, we have

$$f_c = 2\frac{t}{B} - \left(\frac{t}{B}\right)^2, \qquad \text{for the square honeycomb core,}$$

$$f_c = \frac{t}{t + H\cos\alpha}, \qquad \text{for the folded plate core.}$$

The mass/area of the sandwich plate is $M = \rho(2h_f + f_c H)$. If L, M, and ρ are specified, the geometry of each of the sandwich plates is fully determined by f_c, H/L and B/H, or equivalently, by α rather than B/H for the folded plate core.

Following [Rabczuk et al. 2004] and [Liang et al. 2007], two types of clamped boundary conditions will be considered for the sandwich plates: *fully clamped*, where both faces and the webs are welded to rigid supports along the edges; and *periodic bottom clamping*, where only the bottom face is welded to rigid line-supports parallel to the plate. At the support, the top face and the webs are free to deflect in the direction normal to the support but are constrained against tangential displacement and rotation, in accord with periodic support conditions.
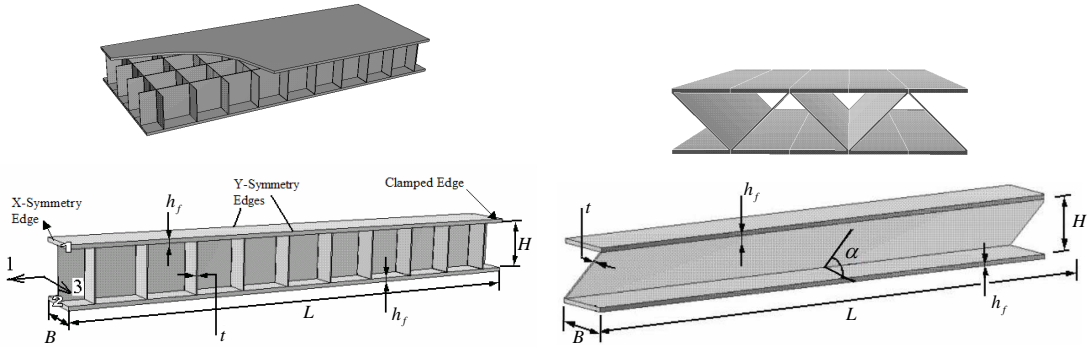
Figure 1. Schematic diagrams of metal sandwich plates configurations and the corresponding computational models for (left) square honeycomb sandwich plate and (right) folded sandwich plate. The width of the plates is $2L$.

The shock loading is modeled by applying a spatially uniform pressure history, $p(t) = p_0 \exp(-t/t_0)$ for $t > 0$, to the surface of the plate towards the blast (the top face), where p_0 and t_0 denote the peak overpressure and decay time associated with shock. In all the calculations presented in this study, $t_0 = 10^{-4}$ s, which is representative of many blast loads and is very short compared to the overall response time of the plates. The impulse/area associated with the applied pressure history is $I = \int_0^\infty p\,dt = p_0 t_0$; to a good approximation, this is the momentum/area transferred to the plate because the impulse associated with the reaction forces at the supports is small over the period in which the shock acts. An alternative way to apply the loading is to assign the initial momentum/area I to the face of the sandwich towards the shock. However, Vaziri and Hutchinson [2007] have shown that the time-dependent pressure pulse gives more realistic predictions, especially for core crush since the crushing occurs early in the deformation history. The effect of fluid-structure interaction can be taken into account, at least approximately, by assigning values to I appropriate to the fluid medium and the mass/area of the face, according to the approach originally proposed for water blasts by Taylor [1963] and developed more fully for sandwich plates by Liang et al. [2007] and as extended recently by Kambouchev et al. [2006] to air blasts.

All calculations were carried out using ABAQUS/Explicit [Hibbit, Karlsson and Sorensen Inc. 2001]. Solid plates are modeled in plane strain and have ten elements through thickness. Full three-dimensional models are constructed for the sandwich plates based on periodic geometric units with detailed meshing of the core as reported more fully in [Xue and Hutchinson 2004] and [Vaziri et al. 2006]. At least four 8-node brick elements were employed through the thickness of each face sheet, which captures early stages of necking with acceptable fidelity. In the calculations, failed elements are removed using the approach available in ABAQUS.

3. Material specifications

Four steels have been selected to span a range of behaviors from a stainless steel (AL6XN) with intermediate yield strength, high strain hardening, and high ductility, to a high strength steel (HY80) with low strain hardening and modest ductility. Also considered are two intermediate strength steels with high ductility (DH36) and low ductility (AH36). The range of behaviors represented by these steels

is used to illustrate some of the critical issues underlying the role of material choice in plate design against impulsive loads. Tensile true stress-logarithmic strain curves for the four materials are presented in Figure 2, left. The effective plastic strain at failure $(\varepsilon_{\text{eff}}^p)_C$ as a function of the triaxiality ratio σ_m/σ_e is plotted for three of the materials in Figure 2, right, where $\sigma_m = \sigma_{kk}/3$ is the mean stress, $\sigma_e = 3s_{ij}s_{ij}/2$ is the effective stress and s_{ij} is the stress deviator. Ductility data for HY80 was not available, but a parametric study will be conducted with this material using the fracture strain as a variable.

A difficulty that must be confronted in any study of this type is the lack of consistent sets of material data available for the different materials. This is even true for basic tensile stress-strain behavior where data incorporating strain-rate dependence is available for some materials and not for others. It is especially true that fracture data that expresses ductility as a function of mean stress is available for only a few materials. Moreover, such data depends on experimental procedures and inferences from specimen analysis that often vary from one investigator to another. In this study, we were forced to confront this difficulty. The data in Figure 2 were taken from various sources, as will now be described.

Young's modulus, Poisson ratio, and the density of all the steel materials mentioned above are taken as $E = 200\,\text{GPa}$, $\nu = 0.3$, and $\rho = 7850\,\text{kgm}^{-3}$. The true stress-plastic strain response and the fracture locus for AH36 are taken from [Wierzbicki and Lee 2005]. For HY80 steel, the true stress-plastic strain response displayed in Figure 2, left, is representative of the material response at tensile strain rate of $100\,\text{s}^{-1}$ as adopted from [Meyer et al. 2000]. Material strain rate dependence is not included for HY80. The tensile data for AL6XN was obtained from [Nahshon et al. 2007] and is similar to that given by [Nemat-Nasser et al. 2001]. For DH36, the Johnson and Cook [1983] plasticity model is employed for representing the stress-strain response of the material, as provided by [Nemat-Nasser and Guo 2003]. Neglecting temperature variations and assuming room temperature, the following relation obtains between the effective stress and effective plastic strain, $\varepsilon_{\text{eff}}^P$:

$$\sigma_e = 470\,\text{MPa}\,\left(1 + 1.5(\varepsilon_{\text{eff}}^P)^{0.4}\right)\left(1 + 0.015\ln(\dot{\varepsilon}_{\text{eff}}^P/1\,\text{s}^{-1})\right),$$
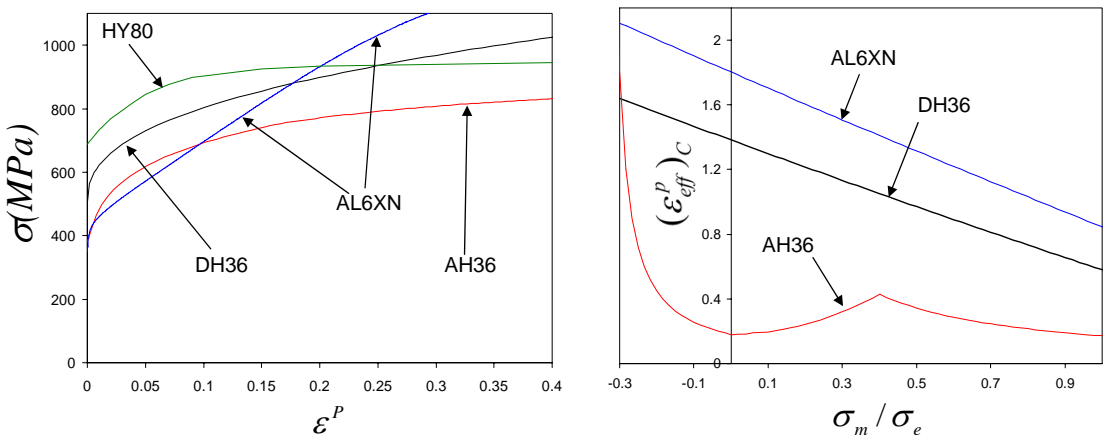

Figure 2. Left: true stress-plastic strain response of the four steels considered in this study. Right: failure locus for three of the four steels.

at the effective strain rate of $\dot{\varepsilon}_{\text{eff}}^{P}$. The stress-strain curve for DH36 at the effective strain rate of

$$\dot{\varepsilon}_{\text{eff}}^{P} = 100\,\text{s}^{-1}$$

is shown in Figure 2, left. The failure locus data for both DH36 and AL6XN are based on fitting experimental data (provided by Edward Johnson, private communication) to the Johnson–Cook shear failure model. Material strain rate dependence is only accounted for in calculations for DH36.

Figure 3 displays the center deflection (the maximum deflection) of solid plates made of the four steels as a function of the peak pressure imparted to the plate, p_0, with impulse period fixed at $t_0 = 10^{-4}$ s. These plates have half-width $L = 1$ m and thickness $h = 20$ mm, corresponding to $M = 157\,\text{kg/m}^2$ and will serve as reference for comparison with equal weight sandwich plates. Over the range of p_0 plotted, the plates of AL6XN, DH36 and HY80 do not fail, because of the extensive ductility assumed for these materials (ductility limits for HY80 will be discussed later). However, plates of AH36 have a clear fracture limit associated with complete separation at edges by the supports. The sharp up-turn of the deflection of the plate made from AH36 just below the complete failure limit at $p_0 \cong 115$ MPa reflects the onset of fracture of the plate precipitated by necking at the plate edges. Once the peak pressure is large enough to cause necking, only slightly larger levels are required to detach the plate. Over the range of peak pressures plotted, a plate of HY80 deflects less than plates made of the other materials due to the higher strength of HY80 over the relevant range of strains (for example, 10 to 15%, as discussed later). The strain hardening and ductility of plates of DH36 and AL6XN ensure survivability to very large deflections, but their lower strength in the relevant range of strains gives rise to larger deflections at a given peak pressure.
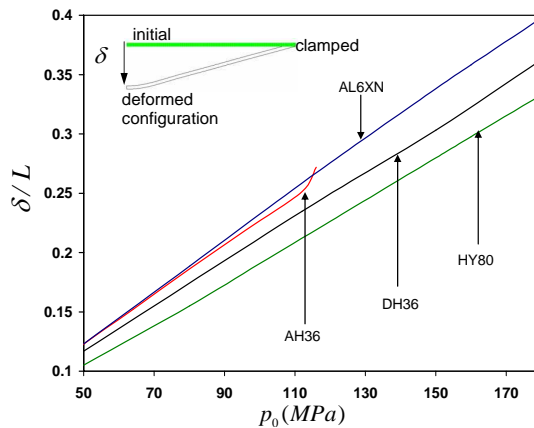

Figure 3. Normalized maximum deflection of solid plates of four steels of thickness 20 mm and width 2 m as a function of peak over-pressure p_0 associated with shock loading. The decay time associated with shock is $t_0 = 10^{-4}$ s. The curve corresponding to the plate made of AH36 is terminated at total failure, where the solid plate separates from the support and undergo free flight, $p_0 \sim 116$ MPa. No total failure is observed for solid plates made from DH36 and AL6XN in the range of peak over-pressure considered in this set of calculations. For HY80 no material failure criterion is incorporated and unlimited ductility has been assumed.

4. Competing fracture modes for sandwich plates of AH36 steel

In this section, we present detailed results on the deformation and failure modes of honeycomb and folded plate core sandwich plates for plates made of AH36 steel. This steel has been chosen for this purpose because the failure strain data is fully characterized and because its lower ductility compared to DH36 and AL6XN highlights the role of fracture limits. Most results have been determined with fully clamped boundary conditions, but a limited set of results will be presented for periodic bottom clamping. All plates have half-width $L = 1$ m and mass/area $M = 157$ kg m^{-2}. As mentioned above, the thickness of the solid plate having the same mass/area is 20 mm, and results for solid plates made from the four steels were presented in the previous section. The core thickness of both types of sandwich plates is fixed at $H/L = 0.1$, and the web spacing of the square honeycomb is fixed at $B/H = 1$ while the folded plate cores have $\alpha = 45°$ such that $B/H \cong 1$. As noted in Section 2, the geometry of both types of sandwich plates is now prescribed by the relative density of the core. The stress-strain data and fracture locus of AH36 presented in Figure 2 were taken from [Wierzbicki and Lee 2005]; the initial yield strength is $\sigma_Y = 380$ MPa. Material strain-rate dependence is not included in the calculations.
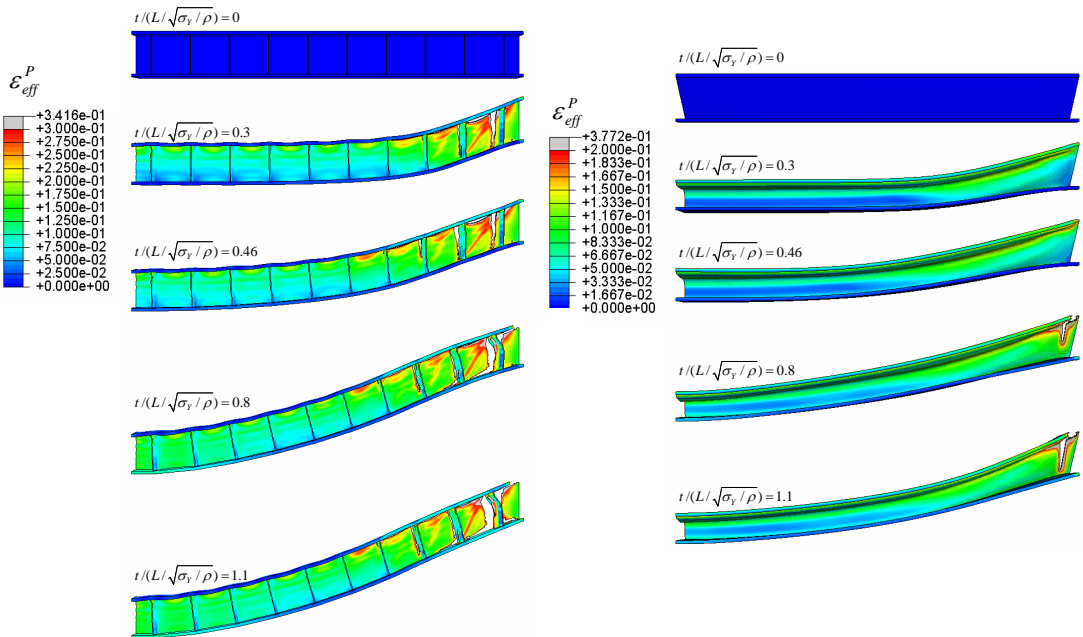

Figure 4. Successive views of the deformed profile at $t/(L/\sqrt{\sigma_Y/\rho}) = 0.0, 0.3, 0.46, 0.8, 1.1$ for (left) a square honeycomb sandwich plate subjected to $p_0 = 128$ MPa ($I/(M\sqrt{\sigma_Y/\rho}) \approx 0.364$) and (right) a folded sandwich plate subjected to $p_0 = 84$ MPa ($I/(M\sqrt{\sigma_Y/\rho}) \approx 0.238$). The sandwich plates have $M = 157$ kg/m^2, $f_c = 0.04$, $L = 1$ m. The decay time associated with shock is $t_0 = 10^{-4}$ s. Equivalent plastic strain field at each successive view is displayed. For both cases, there is no total failure of the sandwich plate since the bottom face remains intact.

4.1. *Fully clamped support conditions.* As reference for the present discussion, we note from Figure 3 that the clamped AH36 solid plate fails by necking, fracture, and finally detachment at the rigid supports at $p_0 \cong 115$ MPa ($I/(M\sqrt{\sigma_Y/\rho}) \approx 0.33$), corresponding to the maximum normalized deflection $\delta/L \approx 0.28$. Figure 4, left, presents successive views at various dimensionless times, $t/(L/\sqrt{\sigma_Y/\rho})$, of the sandwich plate with a square honeycomb core of relative density $f_c = 0.04$ subjected to a shock loading with $p_0 = 128$ MPa ($I/(M\sqrt{\sigma_Y/\rho}) \approx 0.364$). The contour map displays the equivalent plastic strain field at each stage of the response. Figure 4, right, presents the corresponding sequence of deformed states for the plate with a folded plate core with $f_c = 0.04$ and $p_0 = 84$ MPa ($I/(M\sqrt{\sigma_Y/\rho}) \approx 0.238$). For either plate, the applied pressure peaks just below the level required to completely fail the plate, defined as complete separation at the supports. The plate with the square honeycomb core undergoes relatively little core crush in the initial stage of deformation, but then it experiences intense shear in the core webs near the supports. Shear delamination cracks occur along the welds between webs and between the web and the face sheet. As deformation progresses, the top face undergoes tensile necking at the support and then fractures. The plate then comes to rest with the top face and most of the core separated from the support but with the bottom face sheet still intact. For the sandwich plate with the folded plate core, the response differs in several respects, including the occurrence of more extensive core crushing in the first stage and the near-simultaneous failure of the web and the top face sheet at the support. Here, again, the loading intensity is such that the plate comes to rest before the bottom face fails. Fracture begins
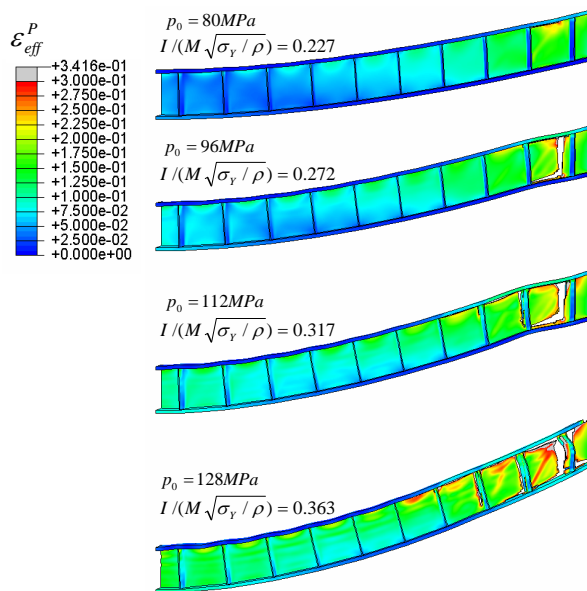

Figure 5. Deformed configurations and the equivalent plastic strain fields of a square honeycomb sandwich plate with the relative core density of, $f_c = 0.04$, subjected to loads of various intensities. The sandwich plates has $M = 157$ kg/m^2 and $L = 1$ m. The decay time associated with shock is $t_0 = 10^{-4}$ s. The equivalent plastic strain field at each deformed configuration is displayed. Even at the highest intensity shown, the bottom face remains intact.

substantially earlier in the plates with the square honeycomb core than in those with the folded plate, due to failures in the core. Nevertheless, the early core fractures are evidently benign: the plate withstands much larger deflections and peak pressures without complete failure.

Figure 5 shows the crack tolerance of the square honeycomb core sandwich plates. The same plate ($f_c = 0.04$) is subjected to four loads of increasing intensity. The figure displays the effective plastic strain distribution and cracks in the plate after it has come to rest. At the lowest loading intensity, plastic shearing occurs in a web near the support and a shear crack has just begun to emerge at the top face sheet. At an impulse that is 20% higher, the crack extends across the web from the top to the bottom face. At the next higher load the crack has spread along the bottom face in the web. At the highest impulse, which is 60% above that causing the first cracks, the top face has detached from the support, but the bottom face remains attached.

Figure 6 reveals the role of the relative density of the core, f_c, for various cases with the same mass/area $M = 157\,\mathrm{kg\,m^{-2}}$. At left, the figure shows the deformed state of the plates with the square honeycomb core, where each has been subjected to an impulse with $p_0 = 96\,\mathrm{MPa}$ ($I/(M\sqrt{\sigma_Y/\rho}) \approx 0.272$). At right are the deformed plates with the folded cores; here the impulse had $p_0 = 84\,\mathrm{MPa}$ ($I/(M\sqrt{\sigma_Y/\rho}) \approx 0.238$). Of the plates with a square honeycomb core, the one with the lowest relative density ($f_c = 0.02$) sustains the largest core crush, and it undergoes extensive shear failure at the core/face weld line. The square honeycomb core plate with the highest relative density ($f_c = 0.08$) undergoes very little core crush, but it nearly fails at the supports. The plate with $f_c = 0.04$ deflects least and exhibits only localized fracture of the core web near the support. The folded-core plate with the lowest relative density ($f_c = 0.02$)
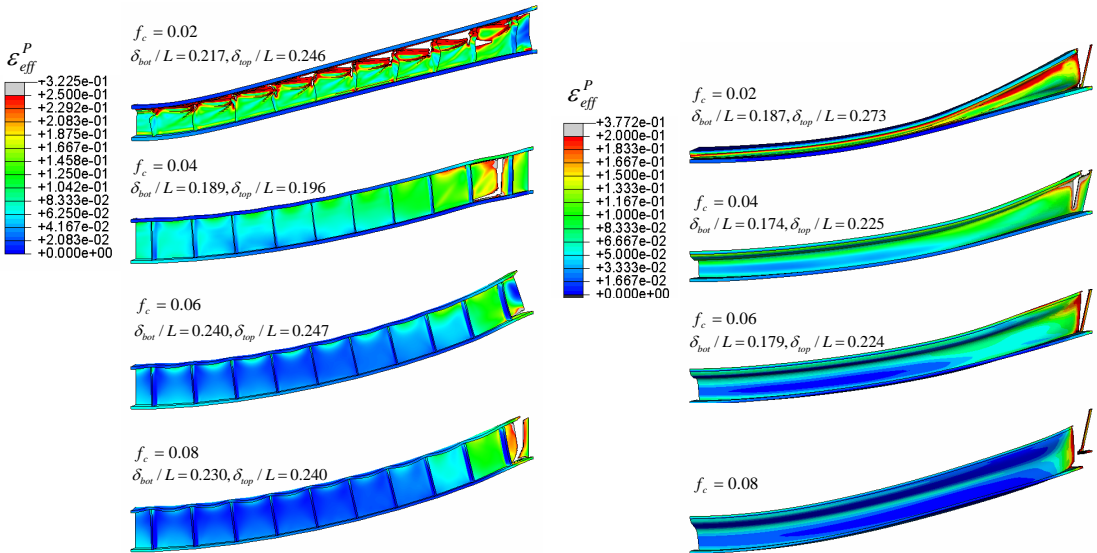

Figure 6. Deformed configurations and the equivalent plastic strain fields of (left) square honeycomb sandwich plates with various core densities subjected to $p_0 = 96\,\mathrm{MPa}$ ($I/(M\sqrt{\sigma_Y/\rho}) = 0.272$) and (right) folded sandwich plates with various core densities subjected to $p_0 = 84\,\mathrm{MPa}$ ($I/(M\sqrt{\sigma_Y/\rho}) = 0.238$). The sandwich plates have $M = 157\,\mathrm{kg/m^2}$ and $L = 1\,\mathrm{m}$. The decay time associated with the loading is $t_0 = 10^{-4}\,\mathrm{s}$.
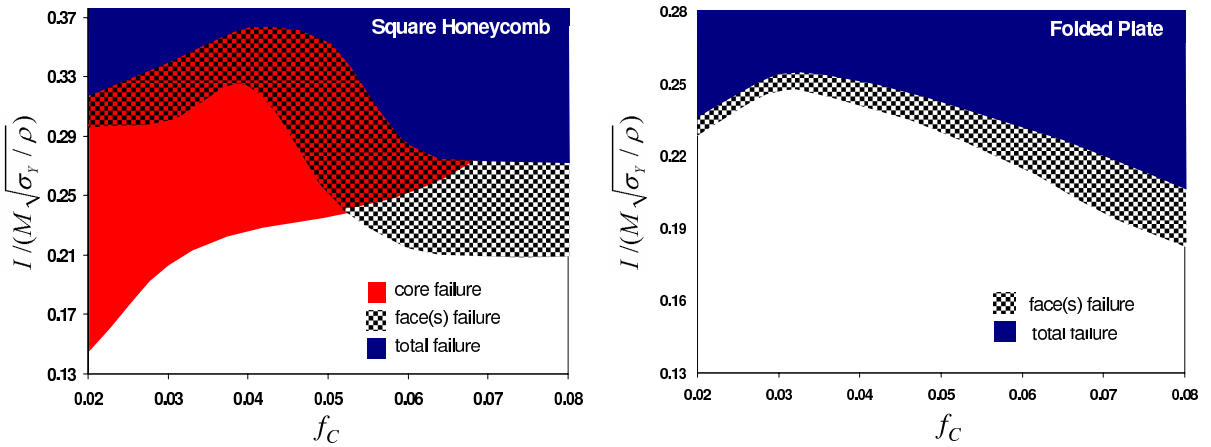
Figure 7. Failure map for square honeycomb and folded sandwich plates as dependent on the relative density of the core. The sandwich plates have $M = 157\,\text{kg/m}^2$ and $L = 1\,\text{m}$. The decay time associated with the loading is $t_0 = 10^{-4}\,\text{s}$.

is completely crushed and fails almost completely at the support. Of all the plates with folded-plate cores, only the one with the highest relative density $f_c = 0.08$ fails completely. The plates with cores of intermediate relative density ($f_c = 0.04$ and $f_c = 0.06$) perform comparably at this level of impulse.

Figure 7 gives failure maps for the sandwich plates as a function of normalized impulse intensity and relative core density. As before, the plates share mass/area $M = 157\,\text{kg m}^{-2}$. In constructing this map, onset of core failure is recognized when the total length of shear delamination becomes equal to the core height. Core failure for the folded-core plates occurs after the failure of the top face at the supports. It is lumped into the total failure region of the plot where the bottom face also fails. By contrast, the honeycomb-core plates have a wide band of core failure if $f_c < 0.06$ at impulse levels well below failure of the two faces. As described above, the sandwich plates fail completely under uniform impulse when both faces and core webs have separated from the supports.

Companion maps in Figure 8 show the maximum deflection of the bottom face sheet. The maximum normalized impulse that can be sustained without total failure is $I/(M\sqrt{\sigma_Y/\rho}) \approx 0.368$ ($p_0 = 130\,\text{MPa}$) for the honeycomb-core plate and $I/(M\sqrt{\sigma_Y/\rho}) \approx 0.258$ ($p_0 = 91\,\text{MPa}$) for the folded-core plate. The largest bottom plate deflections that can be sustained without total failure are $\delta/L \cong 0.3$ for the honeycomb and $\delta/L \cong 0.15$ for the folded.

4.2. *Role of support conditions — fully clamped versus periodic clamping of bottom face.* In this section, a limited set of calculations is presented to study how the edge boundary conditions of a metal sandwich plate affect its overall performance and failure under high intensity loading. We consider square honeycomb and folded sandwich plates made from AH36 steel with relative core density of $f_c = 0.04$. Two idealized boundary conditions are considered.
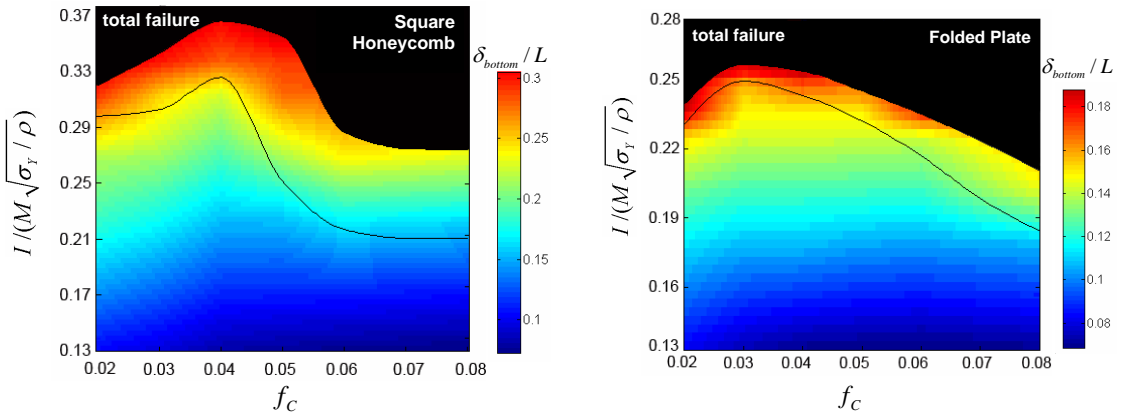
Figure 8. Normalized maximum deflection of the bottom face of (left) square honeycomb sandwich plates and (right) folded sandwich plates as a function of the loading intensity and the relative density of the core. The sandwich plates have $M = 157 \, \text{kg/m}^2$ and $L = 1 \, \text{m}$. The decay time associated with the loading is $t_0 = 10^{-4} \, \text{s}$. The black solid line in each plot corresponds to the top face failure as depicted also in Figure 7.

(i) *Fully clamped.* As above, the edges of both faces and the core webs are welded to rigid supports at the plate ends.

(ii) *Periodic clamping.* The bottom face is welded to rigid supports of zero width. The top face and core webs are free to move perpendicularly to the plate (zero shear traction) but are constrained tangentially.

For both support conditions, Figure 9 displays how the maximum center deflection of each face sheet depends on the normalized loading intensity. The plate has the square honeycomb core. Figure 10 presents similar plots for the sandwich plate with the folded plate core. For comparison, the figure includes the response of the fully clamped solid plate of equal mass from Figure 3. In the fully clamped case, failure of the bottom face constitutes total failure. For periodic clamping, the top face and core webs have not failed when the bottom face tears away at the support. Nevertheless, the damage is extreme when the bottom face fails, and more intense loadings would produce proportionally much larger deflections. For this reason, we believe that the relevant range of intensities has been plotted for periodic clamping.

The plots in Figures 9 and 10 reveal that the support conditions significantly influence how metal sandwich plates respond and fail under high intensity loading. Sandwich plates with periodic clamping experience extensive core crushing at the support. For square honeycomb sandwich plates, the top and bottom faces have comparable center deflections, as relatively little core crushing occurs in the core away from the supports. By contrast, for folded core sandwich plates, the top face sheet undergoes significantly larger center deflections than the bottom face due to core crushing at early stages of deformation. For both types of sandwich plates, the bottom face sheet undergoes significant local stretching which leads to tearing at relatively low intensities of shock load. This effect is more pronounced for the folded sandwich plate, as revealed by comparing the deformed configurations at right in Figures 9 and 10. It is
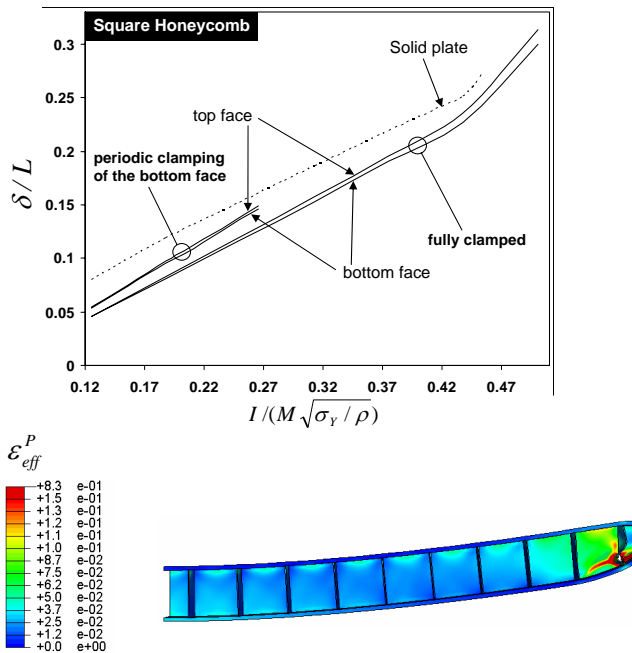
Figure 9. Top: normalized maximum deflection of the solid plate from Figure 2. Normalized maximum deflection of the top and bottom faces of the square honeycomb sandwich plate with $f_c = 0.04$ versus the imparted normalized momentum. Results are shown for two sets of boundary conditions: fully clamped and periodic clamping of the bottom face. The curves are terminated at failure. Bottom: deformed configurations of the square honeycomb sandwich plates with periodic clamping of the bottom face subjected to normalized momentum, $I/(M\sqrt{\sigma_Y/\rho}) = 0.181$. The plate has $M = 157 \, \text{kg/m}^2$ and $L = 1 \, \text{m}$.

noteworthy that the difference between the shock load intensities that cause the two sandwich types to fail is considerably smaller when they are periodically clamped than when they are fully clamped.

Both sets of boundary conditions are idealized in that they assume the plates are welded to immovable supports. It is likely that more realistic modeling of the small support movement may postpone failure of the faces at the supports and allow for larger load intensities to be sustained, particularly for the periodic clamping where support width may be an important factor. The spread of the results in Figures 9 and 10 with support conditions emphasizes that support design is a critical component of effective sandwich plate designs.

5. Comparative performance of sandwich plates made from four steels

In this section, the influence of material properties on the overall response and failure of metal sandwich plates is investigated by considering sandwich plates made from the four steels characterized in Section 3: AH36, DH36, AL6XN and HY80. As emphasized in Section 3, we had to make compromises in conducting this study because of the limited available data. Of the four steels, DH36 is characterized
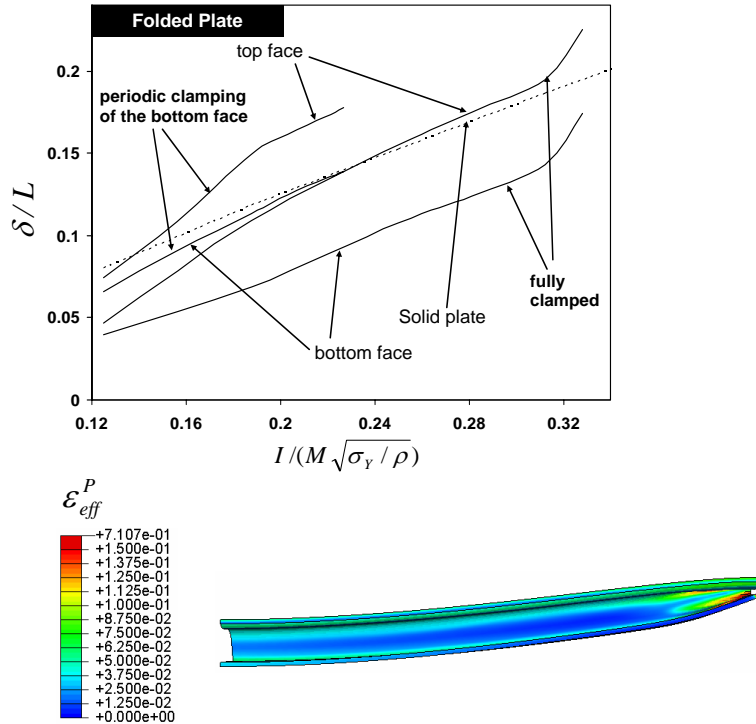
Figure 10. Top: normalized maximum deflection of the solid plate from Figure 2. Normalized deflection of the top and bottom faces of the folded sandwich plate with $f_c = 0.04$ versus the imparted normalized momentum. Results are shown for two sets of boundary conditions: fully clamped and periodic clamping of the bottom face. The curves are terminated at failure. Bottom: deformed configurations of the plates with periodic clamping of the bottom face subjected to normalized momentum, $I/(M\sqrt{\sigma_Y/\rho}) = 0.164$. The plate has $M = 157\,\text{kg/m}^2$ and $L = 1\,\text{m}$.

most completely, and it is the only one for which the strain-rate dependence was incorporated. Concerns about the accuracy of the fracture criteria used for the individual steels have also been noted in Section 3. With these caveats in mind, the comparative study highlights important connections between material properties and plate performance under intense shock loading.

Two specific plate geometries will be considered in this section: the fully clamped sandwich plates analyzed in Section 4 with the square honeycomb core and the folded plate core. Both have relative core density $f_c = 0.04$. The plate dimensions and loading are precisely as specified in Section 4 — only the material is varied.

Figure 11 presents plots of the deflections of the top and bottom faces at the center of the plate as a function of the peak pressure. The left group shows result each of the four steels arranged in plates with a square honeycomb core; at right is the same for folded plate cores. The deflection curves terminate at the peak pressure associated with total failure of the plate, as described earlier. The ductility of DH36 and AL6XN (compare Figure 2, right) is sufficiently large that no failure occurs in either of the two types of plates over the range of blast pressures plotted. By contrast, the limited ductility of AH36 (at least as
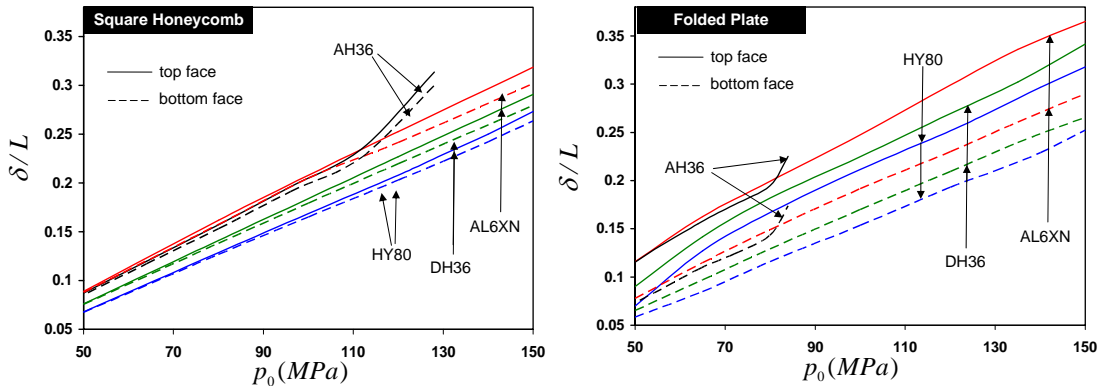
Figure 11. Normalized maximum deflection of top and bottom faces of (left) the square honeycomb and (right) folded sandwich plates with $f_c = 0.04$ for four steels. The results for HY80 assume unlimited ductility. The plates are fully clamped with $M = 157 \, \text{kg/m}^2$ and $L = 1 \, \text{m}$.

assumed for the purposes of this study) leads to failure within the range of blast pressures considered. With no ductility limits assumed for HY80, there is no failure over the range plotted.

Figure 11 also brings out the connection between the strength of the steel and the magnitude of the deflection. At a given peak pressure of the shock loading, plates made from the higher strength steels, HY80 and DH36, sustain smaller deflections than the two lower strength steels, as the scaling relation Equation (1) would suggest. The stretching strength of the faces is important in limiting the deflection, and the effective plastic strain occurring over most of the faces is under 10% for much of the range of deflections shown in Figure 11. Thus, it is the strength of the materials for strains below about 10% that determines the deflection differences seen in Figure 11. That the flow strength of AL6XN exceeds even that of HY80 at strains above 20% (Figure 2, right) reflects the high strain hardening and extensive ductility of AL6XN but has little influence in reducing the overall deflection. For the same reason, strength enhancement due to material rate sensitivity for strains below about 10% is the most important in influencing the deflection. Material rate-dependence for DH36 plays a relatively small role in determining the overall deflection. The elevation in flow stress for a strain rate on the order of $100 \, \text{s}^{-1}$, which is relevant to the dynamic plate response, is only about 5% above that associated with low strain rates, with deflection reductions scaling as in Equation (1).

Further insight into failure development in the HY80 sandwich plates is provided by Figure 12, top, which presents the effective plastic strain, averaged through the face thickness at the point along the top face where it is largest, as a function of the shock peak pressure. The corresponding result for the solid plate having the same mass is also included. These results have been computed assuming unlimited ductility for the HY80. For peak pressures below 120 MPa, the maximum plastic strain in the top face of the square honeycomb core plate occurs at the support, and the magnitude is close to that of the solid plate. Plastic shear strains in the core webs are considerably larger than the strains in the top face at this stage. For $p_0 > 120 \, \text{MPa}$, the location of the maximum plastic strain in the face shifts inward from the support (Figure 12, bottom left). There is an associated steep increase in the maximum strain caused by increasing blast intensity associated with necking at this location. The critical location for the face
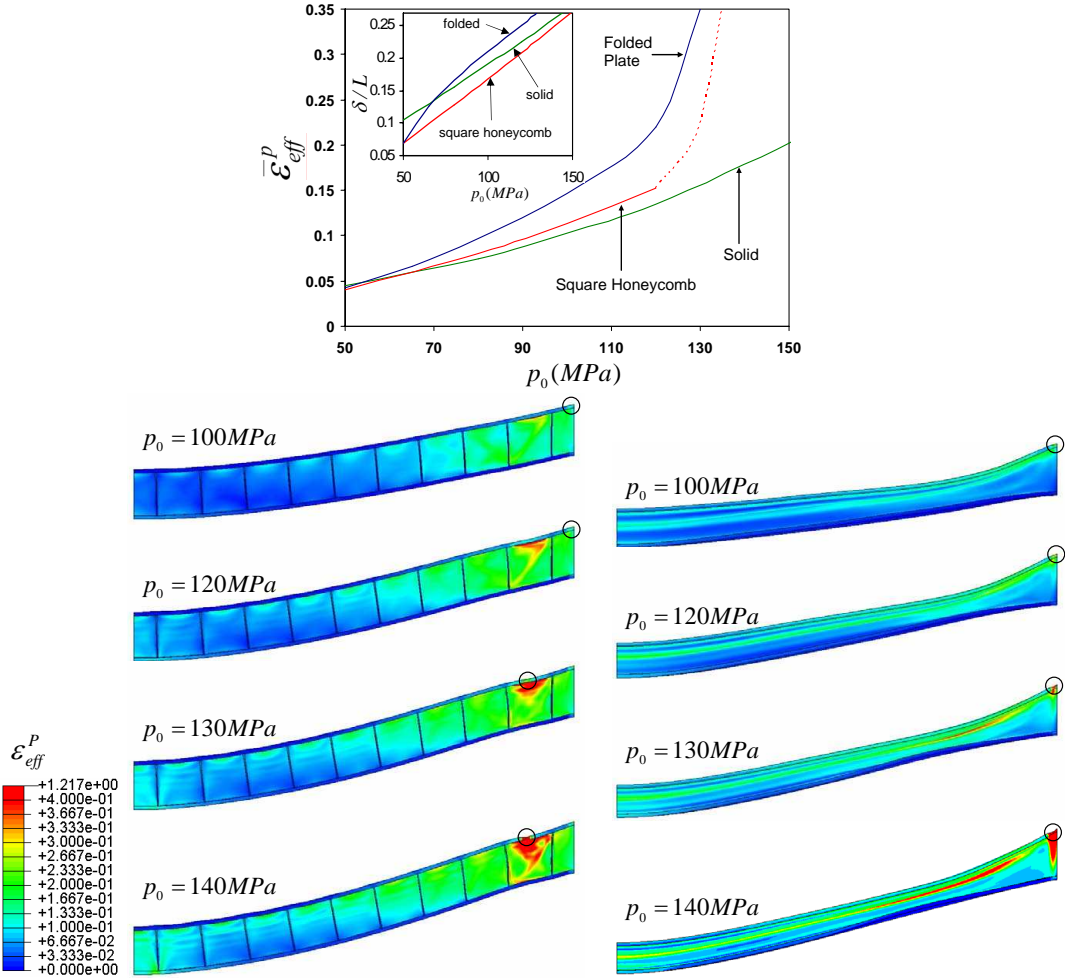
Figure 12. Strains in plates of HY80 and $f_c = 0.04$ computed assuming unlimited ductil-
ity. Top: effective plastic strain averaged through the thickness of the top face sheet at the
location where it is the maximum. The result for the solid plate is included. The decay
time associated with the loading is $t_0 = 10^{-4}$ s. The inset shows the normalized deflection
as a function of the load intensity. Bottom left and right: deformed configurations of the
square honeycomb and folded sandwich plates at various levels of peak over-pressure.
The location of maximum equivalent plastic strain in the top face is indicated by black
circles on each deformed configurations. The plates have $M = 157 \, \text{kg/m}^2$ and $L = 1$ m.

of the folded core sandwich plate is at the support (Figure 12, bottom right), where necking sets in at
approximately the same loading intensity as for the square honeycomb plate. Intense plastic shearing
also occurs in the core webs of this plate.

To illustrate the role of ductility for HY80, a series of studies has been carried out for the square
honeycomb plate analyzed in Figure 12, top and bottom left, (with $f_c = 0.04$) treating the fracture strain
$(\varepsilon_{\text{eff}}^P)_c$ as a parameter. As mentioned earlier in the paper, fracture data on HY80 was not available. As a
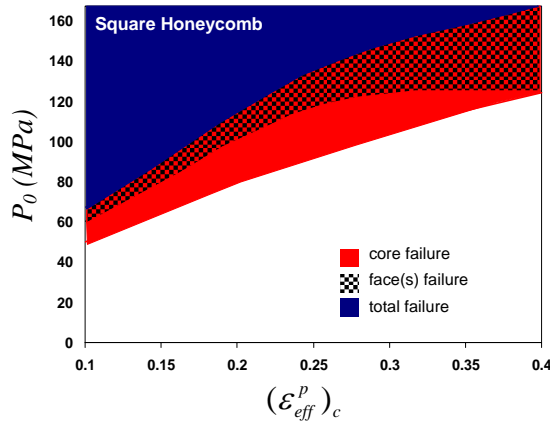
Figure 13. The failure map for HY80 as dependent on the critical effective plastic strain at fracture. $(\varepsilon_{\text{eff}}^P)_c$ is taken to be independent of mean stress. Square honeycomb core plates with $M = 157\,\text{kg/m}^2$, $L = 1\,\text{m}$ and $f_c = 0.04$.

high-strength steel, HY80 is expected to have limited ductility and its fracture strain is likely to depend on stress triaxiality. In the present simulations, $(\varepsilon_{\text{eff}}^P)_c$ will be taken as independent of triaxiality given the absence of data, but we will comment on what effect it might have had in what follows. A fracture diagram delineating core fractures, top face failure, and total failure as a function of blast intensity p_0 is shown in Figure 13 for fracture strains $(\varepsilon_{\text{eff}}^P)_c$ ranging from 0.1 to 0.4.

For the lowest fracture strain, $(\varepsilon_{\text{eff}}^P)_c = 0.1$, the plate undergoes total failure at a surprisingly low intensity ($p_0 \cong 70\,\text{MPa}$). The sequence of events leading to total failure is shear failure where the core webs are joined to the top face, followed by progressive failure of the top face, and finally necking and tearing of the bottom face at the sheet. The sequential nature of the failure significantly reduces the maximum intensity the plate can withstand compared with a prediction computed by assuming no intermediate failures and by applying the critical strain criterion to the bottom face (compare Figure 12). Thus, for example, if the critical strain in shear (a low triaxiality stress state) were much higher than 0.1, then the core webs would not fail first in shear and the maximum sustainable pressure would likely be considerably larger than $p_0 \cong 70\,\text{MPa}$. In Figure 13, a HY80 fracture strain, $(\varepsilon_{\text{eff}}^P)_c \cong 0.35$, is required to sustain intensities in the upper range of those plotted in Figure 11, that is, $p_0 \cong 140\,\text{MPa}$. A fracture strain this large seems unlikely for steels with the high strength and low strain hardening of HY80. Another feature of note in Figure 13 is that top face failure becomes independent of fracture strain for $(\varepsilon_{\text{eff}}^P)_c > 0.25$, implying necking localization itself constitutes failure. In addition, for $(\varepsilon_{\text{eff}}^P)_c > 0.4$, the top face fails before the core fractures.

6. Conclusions

Sandwich plates made of four steels and subjected to impulsive pressure loads have been simulated to learn how plate deflection and the fracture modes depend on load intensity. The materials range from relatively low strength steels with high strain hardening and ductility to high strength steels with low strain hardening. As emphasized in the paper, some of the fracture properties obtained from the literature

for the materials may be suspect. Whether hypothetical or not, the fracture properties serve to illustrate the trade-off between strength and ductility in the design of high performance steel sandwich plates. In particular, high strength reduces plate deflections and is beneficial as long as fracture does not occur. However, face sheets of high strength steel with low strain hardening, such as HY80, are susceptible to necking as they stretch, which is followed soon thereafter by face sheet tearing. By contrast, plates made of DH36 steel are not as strong as those of HY80 and deflect somewhat more in the range of load intensities in which both plates survive. Due to their extensive ductility, plates of DH36 and AL6XN did not fail over the range of deformations and load intensities considered here.

This paper has emphasized fractures that develop in a plate subjected to a single blast load and examined their extent as a function of blast intensity. It did not study the residual capacity of the plate after it has been damaged; however, the methods used here are capable of addressing the residual strength and blast resistance.

The damage tolerance appears to differ between plates with square honeycomb cores and those with folded plate cores (Figure 7). Local fractures and delaminations of the honeycomb web occur at load intensities well below the intensity that causes total failure of the plate. On the other hand, in plates with folded plate cores, the core fractures in a narrow range of load intensities just below the intensity at total failure. For a material with fracture properties such as those assumed for AH36 steel, the honeycomb-core plates can sustain significantly more load intensity than those with folded plate cores. In this connection, it is important to recognize that the load intensity applied to the plate, as measured here by either the peak pressure p_0 or the impulse/area, doesn not account for any fluid-structure interaction. Thus, for water blasts, it is generally not valid to make a direct comparison between square honeycomb and folded plate core performances based on the same p_0 since fluid-structure interaction for the two cores is different.

A limited study of the role of support conditions has been conducted by comparing behavior under fully clamped conditions with those where the plate is a periodic unit that is supported only at the bottom face away from the blast. The results suggest that the latter means of support is more susceptible to fracture and cannot sustain as much load intensity as the fully clamped plate, at least to the point where the bottom face fails. The most important conclusion to be drawn from this limited comparison is that support details are very important in the design of sandwich plates against intense dynamic loads.

References

[Fleck and Deshpande 2004] N. A. Fleck and V. S. Deshpande, "The resistance of clamped sandwich beams to shock loading", *J. Appl. Mech.* (*Trans. ASME*) **71** (2004), 386–401.

[Hancock and Mackenzie 1976] J. W. Hancock and A. C. Mackenzie, "On the mechanisms of ductile failure in high-strength steels subjected to multi-axial stress states", *Journal of Mechanics and Physics of Solids* **24** (1976), 1471–69.

[Hibbit, Karlsson and Sorensen Inc. 2001] Hibbit, Karlsson and Sorensen Inc., *ABAQUS/Explicit User's Manual*, Hibbit, Karlsson and Sorensen Inc., 2001. Version 6.0.

[Hutchinson and Xue 2005] J. W. Hutchinson and Z. Xue, "Metal sandwich plates optimized for pressure impulses", *Int. J. Mech. Sci.* **47** (2005), 545–569.

[Johnson and Cook 1983] G. R. Johnson and W. H. Cook, "A constitutive model and data for metals subjected to large strains, high strain rates and high temperatures", pp. 541–547 in *Proceedings of 7th International Symposium On Ballistics*, Netherlands, 1983.

[Kambouchev et al. 2006] N. Kambouchev, L. Noels, and R. Radovitzky, "Compressibility effects in fluid-structure interaction and their implications on the air-blast loading of structures", *J. Appl. Phys.* **100** (2006), 063519.

[Liang et al. 2007] Y. Liang, A. V. Spuskanyuk, S. E. Flores, D. R. Hayhurst, J. W. Hutchinson, R. M. McMeeking, and A. G. Evans, "The response of metal sandwich panels to water blasts", *J. Appl. Mech.* (*Trans. ASME*) **74** (2007), 81–99.

[Meyer et al. 2000] L. W. Meyer, L. Krüger, and F. F. Hahn, "Influence of pre-deformation and strain rate on the flow behavior of HY80 steel", pp. 295–300 in *Pressure vessels and piping*, vol. 414, Emerging technologies in fluids, structures and fluid/structure interactions **1**, 2000.

[Nahshon et al. 2007] K. Nahshon, M. G. Pontin, A. G. Evans, J. W. Hutchinson, and F. W. Zok, "Dynamic shear rupture of steel plates", *Journal of Mechanics of Materials and Structures* (2007). In press.

[Nemat-Nasser and Guo 2003] S. Nemat-Nasser and W. Guo, "Thermomechanical response of DH-36 structural steel over wide range of strain rates and temperatures", *Mech. Mater.* **35** (2003), 1023–1047.

[Nemat-Nasser et al. 2001] S. Nemat-Nasser, D. P. Kihl, and W. Guo, "Thermomechanical response of AL-6XN stainless steel over a wide range of strain rates and temperatures", *Journal of Mechanics and Physics of Solids* **49** (2001), 1823–1846.

[Rabczuk et al. 2004] T. Rabczuk, J. Y. Kim, E. Samaniego, and T. Belytschko, "Homogenization of sandwich structures", *Int. J. Numer. Methods Eng.* **61** (2004), 1009–1027.

[Taylor 1963] G. I. Taylor, "The pressure and impulse of submarine explosion waves on plates", pp. 287–303 in *The scientific papers of Sir Geoffrey Ingram Taylor, volume III: aerodynamics and the mechanics of projectiles and explosions*, edited by G. K. Batchelor, Cambridge University Press., 1963.

[Vaziri and Hutchinson 2007] A. Vaziri and J. W. Hutchinson, "Metal sandwich plates subject to intense air shocks", *Int. J. Solids Struct.* **44** (2007), 2021–2035.

[Vaziri et al. 2006] A. Vaziri, Z. Xue, and J. W. Hutchinson, "Metal sandwich plates with polymeric foam-filled cores", *Journal of Mechanics of Materials and Structures* **1** (2006), 95–128.

[Wierzbicki and Lee 2005] T. Wierzbicki and Y. W. Lee, "Fracture prediction of thin plates under localized impulsive loading. Part II: discing and petalling", *Int. J. Impact Eng.* **31** (2005), 1277–1308.

[Xue and Hutchinson 2004] Z. Xue and J. W. Hutchinson, "A comparative study of impulse-resistant metallic sandwich plates", *Int. J. Impact Eng.* **30** (2004), 1283–1305.

ASHKAN VAZIRI: avaziri@seas.harvard.edu
School of Engineering and Applied Sciences, Harvard University, Cambridge, MA 02138, United States
www.seas.harvard.edu/~avaziri

ZHENYU XUE: xue@esag.harvard.edu
School of Engineering and Applied Sciences, Harvard University, Cambridge, MA 02138, United States

JOHN W. HUTCHINSON: hutchinson@husm.harvard.edu
School of Engineering and Applied Sciences, Harvard University, Cambridge, MA 02138, United States
http://www.seas.harvard.edu/hutchinson/